Temperature and Strain Sensors Based on Integration of Tilted Fiber Bragg Gratings With a Free Spectral Range Matched Interrogation System

Somayyeh Rahimi, Dayan Ban, *Member, IEEE*, Gaozhi Xiao, Zhiyi Zhang, and Jacques Albert

***Abstract*—In this work, a tilted fiber Bragg grating (TFBG) is integrated with a free spectral range matched interrogation (FSRMI) system for temperature and strain sensing applications. The experimental data show that the peak wavelengths of the core and cladding modes of the TFBG shift linearly to longer wavelength with the increase of temperature and strain. Since the FSRMI system allows simultaneous demodulation of multiple wavelengths, the sensing system can be extended by integrating a n-channel FSRMI with n TFBGs for multipoint temperature and strain sensing with high precision and fast detection rate.**

***Index Terms*—Free spectral range matched interrogation (FSRMI), multiple-point sensing, temperature and strain sensor, tilted fiber Bragg grating sensors.**

I. Introduction

IN-FIBER Bragg gratings (FBGs) have been of substantial interests due to their numerous applications in strain, temperature, magnetic field, and in-line reflection sensing [1]–[8]. Among them titled fiber Bragg gratings (TFBGs) are short-period gratings where the refractive index modulation of the core is purposely blazed with respect to the fiber axis by a tilt angle in order to enhance coupling between the forward-propagating core mode and the contra-propagating cladding modes. The core mode resonance and cladding mode resonances of a TFBG appear as multiple dips in the transmission spectrum. The resonance wavelengths are sensitive to differential changes in tilt angle, refractive index of the surrounding and environmental parameters [9], [10], TFBGs have therefore been used for temperature and strain sensing applications. A few commonly used wavelength demodulation approaches include wavelength-division multiplexing (WDM) interrogation techniques, charge-coupled devices (CCD) interrogation techniques, fiber Fabry–Pérot (FFP) filter interrogation techniques and others [11]–[14]. The WDM techniques and the CCD techniques are used due to their high precision and fast response time. However, they could be costly for simple applications. Conventional FFP filter techniques are typically operated in a non-free-spectral-range-matched scheme, and thus can hardly be operated at frequencies higher than a few Kilohertz. For real-time environmental and structural stability monitoring that has to be done at multiple locations and needs to correlate the measurements with each other, a fast interrogation of multiple wavelengths with a portable, low-cost and high-precision system is highly desired [15]. In this paper, a free spectral range matched interrogation (FSRMI) system is deployed to demodulate the wavelength shift of a TFBG under different temperature and strain conditions. Due to its capability of demodulating multiple wavelengths simultaneously, the FSRMI system can be integrated with TFBGs for multiple-point sensing applications. The transmission spectra of the TFBG are measured using the FSRMI system and the temperature coefficient and strain coefficient of the core and cladding modes of the TFBG are derived. Our results demonstrate an integrated FSRMI and TFBG system for temperature and strain sensing application. This will lead to a cost-effective, fast-response, and multiple-channel sensing system toward industrial applications such as multipoint, compact, high sensitive temperature, and strain sensors.

II. Experimental Setup

The FSRMI system consists of an electrically tunable FFP filter and a multichannel bandpass filter followed by photodetectors (Fig. 1). Input optical signal is launched into the tunable FFP filter (Micron Optics, FFP-TF2). The output from the FFP filter is then directed into the multichannel bandpass filter and the optical signal is split into different channels and is converted to electrical signal by the photodetectors. The electrical signal is acquired by a personal computer for subsequent data storage, processing and display. The detected signal intensity (I) is proportional to the overlap among incoming optical spectrum ($R(\lambda)$), the FFP filter transmission spectrum ($F(\lambda)$), and the bandpass filter transmission spectrum ($B(\lambda)$): $I \propto \int R(\lambda)F(\lambda)B(\lambda)d\lambda$. The bandpass filter transmission spectrum $B(\lambda)$ remains constant in each of its transmission channels ($\lambda_a < \lambda < \lambda_b$), which are chosen to match the free spectral range of the tunable FFP filter. The transmission spectrum $F(\lambda)$ of the FFP filter can be approximated as a delta-like function in each corresponding free spectral range

Manuscript received December 02, 2008; revised January 19, 2009; accepted February 04, 2009. Current version published June 19, 2009. This work was supported in part by the University of Waterloo and the Institute for Microstructural Sciences (IMS), National Research Council of Canada (NRC). The associate editor coordinating the review of this paper and approving it for publication was Prof. Francisco Arregui.

S. Rahimi is with the Department of Electrical and Computer Engineering, University of Waterloo, Waterloo, ON N2L 3G1, Canada, and the Institute for Microstructural Sciences, National Research Council of Canada, Ottawa, ON K1A 0R6, Canada (e-mail: srahimi@uwaterloo.ca).

D. Ban is with the Department of Electrical and Computer Engineering, University of Waterloo, Waterloo, ON N2L 3G1, Canada (e-mail: dban@uwaterloo.ca).

G. Xiao and Z. Zhang are with the Institute for Microstructural Sciences, National Research Council of Canada, Ottawa, ON K1A 0R6, Canada (e-mail: george.xiao@nrc-cnrc.gc.ca; Zhiyi.zhang@nrc-cnrc.gc.ca).

J. Albert is with the Department of Electronics, Carleton University, Ottawa, ON K1S5B6, Canada (e-mail: jalbert@doe.carleton.ca).

Digital Object Identifier 10.1109/JSEN.2009.2024710

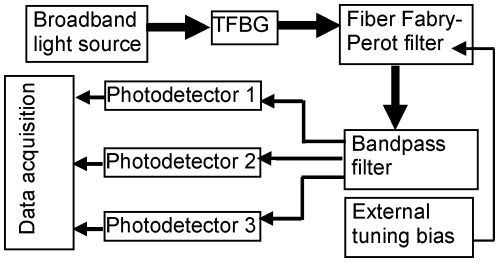

Fig. 1. Block diagram of the experimental setup which integrates a TFBG and an FSRMI system. The diagram shows a multichannel ($n = 3$) bandpass filter. The FFP filter is tuned by applying an external dc bias. The tunable FFP filter is manufactured by Micro Optics (FFP-TF2). The bandpass filter is manufactured by Opto-Link (C-Band, four channels). The photodetctors are manufactured by EG & G Company (FD-InGaAs).

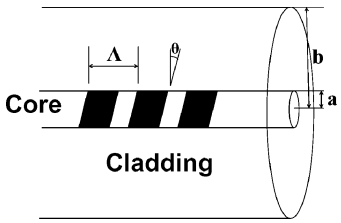

Fig. 2. Schematic diagram of a Tilted fiber Bragg Grating. Λ: grating period, and θ: tilt angle (blaze angle).

($\lambda_a < \lambda < \lambda_b$). The detected signal ($I$) is therefore proportional to the incoming spectrum ($R(\lambda)$).

The free spectral range of the tunable FFP filter is 4.0 nm, so is the bandwidth of each channel of the bandpass filter. An external voltage is applied to the FFP filter to scan the peak wavelengths of its delta-like transmission modes. A wavelength shift of 5 pm is obtained with an incremental step of 0.02 V of the external voltage bias. The maximum sampling rate attainable with the system is three mega samples per second. The number of photodetectors is the same as the number of channels of the bandpass filter. An n-channel FSRMI allows simultaneous scanning and thus improvement of detection speed by n times comparing to a non-free-spectral-range-matched interrogation scheme. This technique can provide solutions for wavelength demodulation of multisensor arrays with high sampling speed and wavelength resolution.

Fig. 2 shows a schematic of the cross section of a TFBG. The TFBGs exhibit to have the ability to couple the light from the core of the fiber to the cladding at numerous discrete wavelengths shorter than the Bragg wavelength. Two resonance modes in TFBGs, called Bragg and Ghost modes, are generally more attractive for sensing purposes. The Bragg mode results from the interference between the forward-propagating core mode and contra-propagating core mode, while the Ghost mode from the interference between the forward-propagating core mode and the first contra-propagating cladding mode. The Bragg and Ghost resonance wavelengths are determined by a phase-matching condition and can be given by the following equations [16]:

$$\lambda_{\text{Bragg}} = \frac{2n_{\text{eff,core}}\Lambda}{\cos\theta} \tag{1}$$

$$\lambda_{\text{Ghost}} = \frac{(n_{\text{eff,cladding1}} + n_{\text{eff,core}})\Lambda}{\cos\theta} \tag{2}$$

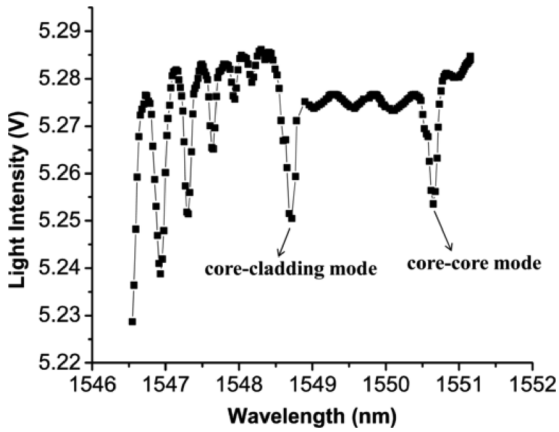

Fig. 3. Transmission spectrum of the TFBG with a tilt angle of 6° measured using the FSRMI system. The turning voltage applied to the FFP filter is converted to wavelength using a precalibrated conversion table. The Bragg mode (core–core mode) is at 1550.576 nm. The Ghost mode (core–cladding mode) is at 1548.416 nm.

where $n_{\text{eff,cladding1}}$ and $n_{\text{eff,core}}$ are the effective refractive index of the ghost mode and core mode, respectively, and Λ is the grating period and θ is the tilt angle (blaze angle). The TFBGs used in this research are written in the hydrogen-loaded Corning SMF-28 fibers using a KrF excimer laser ($\lambda = 248\ \text{nm}$). A phase mask is employed to generate the grating pattern. The mean optical power is kept constant and the gratings are inscribed with a single sweep of the UV laser along the phase mask with a velocity of the order of 10 $\mu\text{m/s}$. After the inscription process the gratings are annealed at 100 °C for a few hours.

III. Results and Discussion

Fig. 3 shows the transmission spectrum of the TFBG with a tilt angle of 6° that is measured using the FSRMI system. The TFBG is under no strain and at room temperature. Two channels of the FSRMI system are employed to scan simultaneously in 30 seconds over the wavelength ranges of [1546-1550] and [1550-1554] nm, in which the Ghost and Bragg modes are located, respectively. The Bragg and Ghost modes are identified in Fig. 3 at 1550.576 and 1548.416 nm, respectively. Other resonance dips at the shorter wavelength side are attributed to the interference between the forward-propagating core mode and higher order contra-propagating cladding modes.

The Bragg and Ghost resonance wavelengths depend on environmental parameters such as temperature and strain. To examine the effect of strain, two ends of the TFBG are mounted to two optical translation stages, respectively. By changing the distance between the two stages, the strain that is applied on the TFBG can be adjusted. The strain is defined as the relative change of the length of the fiber $\Delta l/l$ and is usually measured in the unit of $\mu\varepsilon$. 1 $\mu\varepsilon$ is a strain that changes a 1-meter-long fiber by 1 μm. The transmission spectra of the TFBG are measured under different strain conditions using the FSRMI system. It shows that the general form of the transmission spectra stays almost the same but the Bragg and Ghost resonance wavelengths drift linearly with the increase of the strain.

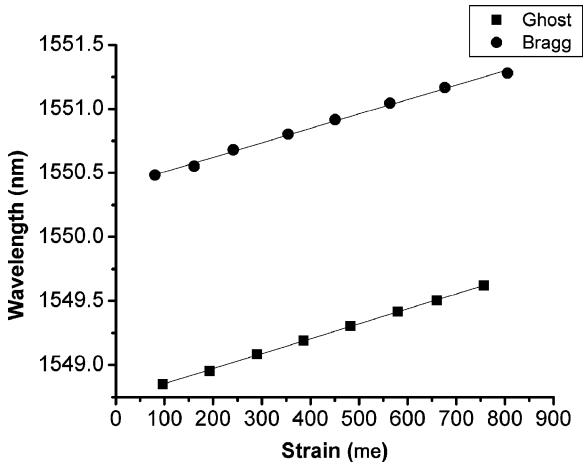

Fig. 4. The Bragg and Ghost resonance wavelengths of the TFBG as a function of strain at room temperature. The TGBG has a tilt angle of 6°.

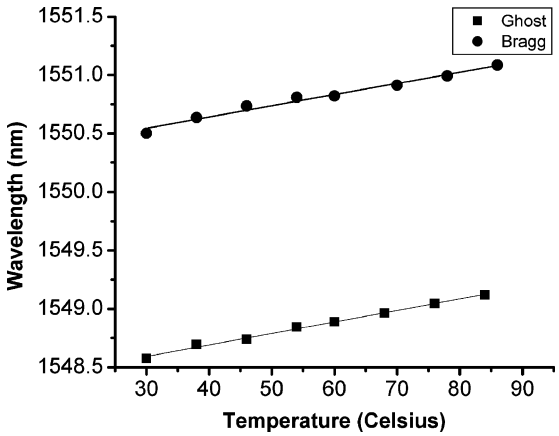

Fig. 5. The Bragg and Ghost resonance wavelengths of the TFBG as a function of temperature under zero strain. The TGBG has a tilt angle of 6°.

Fig. 4 shows the shift of the Bragg and Ghost resonance wavelengths as a function of the strain. The TFBG is kept constant at room temperature so the wavelength variation due to temperature effect is negligible. Both the Bragg and Ghost resonance wavelengths shift to longer wavelengths upon the application of the external strain to the TFBG and a linear relationship is observed. This can be explained by the fact that the grating period (Λ) of the TFBG increases as a result of stretching the fiber (the strain). The increase of Λ is proportional to the strain ($\Delta l/l$) and the resonance wavelengths are proportional to the grating period Λ [(1) and (2)], as a result, the Bragg and Ghost resonance wavelengths shift linearly with the increase of the strain. From the slopes of the two curves in Fig. 4, the strain coefficients of the TFBG for the Bragg and Ghost modes are derived as $K_{B\varepsilon} = 1.13\,\mathrm{pm}/\mu\varepsilon$ and $K_{G\varepsilon} = 1.17\,\mathrm{pm}/\mu\varepsilon$, respectively.

The temperature effect is also examined by measuring the transmission spectra of the TFBG under different temperatures and the results are plotted in Fig. 5. The temperature of the TFGB is tuned from room temperature up to around 100 °C and each of the temperatures is controlled within 1 °C. The TFGB is under zero strain in the measurements. The Bragg and Ghost resonance wavelengths shift linearly with the increase of temperature. This is attributed to the thermal expansion of the fiber, which lead to the linear increase of the grating period. The temperature coefficient of the Bragg and Ghost modes are derived from the slopes in Fig. 5 as $K_{BT} = 9.59\,\mathrm{pm/°C}$ and $K_{GT} = 9.84\,\mathrm{pm/°C}$ over the temperature range from room temperature to around 100 °C.

In practical applications, both strain and temperature induced wavelength shifts of the Bragg and Ghost modes need to be counted. The response due to the variation of strain and temperature may be expressed in terms of a matrix [(3)], the inverse of which would be used to determine independently temperature change (ΔT) and strain change ($\Delta\varepsilon$) given that the strain and temperature coefficients of the Bragg mode are adequately distinct from those of the Ghost mode. For this purpose, specially designed TFBGs need to be fabricated

$$\begin{pmatrix} \Delta\lambda_{\mathrm{core}} \\ \Delta\lambda_{\mathrm{cladding}} \end{pmatrix} = \begin{pmatrix} K_{B\varepsilon} & K_{BT} \\ K_{G\varepsilon} & K_{G\varepsilon} \end{pmatrix} \begin{pmatrix} \Delta\varepsilon \\ \Delta T \end{pmatrix}. \tag{3}$$

The FSRMI system is capable of discriminating a wavelength shift of 5 pm when the FFP filter is set to have a tuning voltage with an incremental step of 0.02 V. As a result, the minimum temperature variation and strain variation that can be distinguished by the integrated FSRMI-TFBG system is estimated to be ~ 0.5 °C and $\sim 5\ \mu\varepsilon$, which is sufficient for practical applications in environmental monitoring and structure stability studies.

IV. Conclusion

This work presents experimental results of using a new approach to interrogate a tilted fiber Bragg grating sensor. This FSRMI technique employs a high finesse, narrow linewidth, tunable FFP filter to achieve a high wavelength resolution. In combination with an n-channel bandpass filters that have transmission bandwidth matched to the free spectral range of the FFP filter, the system ensures fast scanning rate which can be n times faster than a non-free-spectral-range-matched approach. The temperature and strain dependence of the Bragg and Ghost resonance wavelength shifts are measured using this FSRMI technique. The experimental study shows the potential of the integrated system of the new FSRMI technique and tilted fiber Bragg gratings for multipoint, multichannel temperature and strain sensors with low cost, high sensitivity, and high speed.

Acknowledgment

The author S. Rahimi would like to thank the staffs at the Institute for Microstructural Sciences (IMS), National Research Council of Canada (NRC), for their tremendous support. D. Ban thanks Dr. Z. G. Lu for technical support.

References

[1] A. D. Kersey, M. A. Davis, H. J. Patrick, M. LeBlane, K. P. Koo, C. G. Askins, M. A. Putnam, and E. J. Friebele, "Fiber grating sensors," *J. Lightw. Technol.*, vol. 5, no. 8, pp. 1442–1463, 1997.

[2] E. Chehura, S. W. James, and R. P. Tatam, "Simultaneous independent measurement of temperature and strain using a tilted fibre Bragg grating," in *Proc. SPIE*, 2007, vol. 6619, pp. 66190I-1–4.

[3] S. C. Kang, S. Y. Kim, S. B. Lee, S. W. Kwon, S. S. Choi, and B. Lee, "Temperature-independent strain sensor system using a tilted fiber Bragg grating demodulator," *IEEE Photon. Technol. Lett.*, vol. 10, pp. 1461–1463, 1998.

[4] O. Frazao, L. A. Ferreira, F. M. Araujo, and J. L. Santos, "Applications of fiber optic grating technology to multi-parameter measurement," *Fibre Int. Opt.*, vol. 24, pp. 227–244, 2005.
[5] P. M. Cavaleiro, F. M. Araujo, L. A. Ferreira, J. L. Santos, and F. Farahi, "Simultaneous measurement of strain and temperature using Bragg gratings written in germanosilicate and boron-codoped germanosilicate fibers," *IEEE Photon. Technol. Lett.*, vol. 11, pp. 1635–1637, 1999.
[6] X. W. Shu, D. H. Zhao, L. Zhang, and I. Bennion, "Use of dual-grating sensors formed by different types of fiber Bragg gratings for simultaneous temperature and strain measurements," *Appl. Opt.*, vol. 43, pp. 2006–2012, 2004.
[7] C. Ambrosino, S. Campopiano, A. Cutolo, and A. Cusano, "Sensitivity tuning in Terfenol-D based fiber Bragg grating magnetic sensors," *IEEE Sensors J.*, vol. 8, pp. 1519–1520, 2008.
[8] P. Tsai, F. Sun, G. Xiao, Z. Zhang, S. Rahimi, and D. Ban, "A new fiber-Bragg-grating sensor interrogation system deploying free-spectral-range-matching scheme with high precision and fast detection rate," *IEEE Photon. Technol. Lett.*, vol. 20, pp. 300–302, 2008.
[9] C. Caucheteur and P. Megret, "Demodulation technique for weakly tilted fiber Bragg grating refractometer," *IEEE Photon. Technol. Lett.*, vol. 17, pp. 2703–2705, 2005.
[10] S. Baek, Y. Jeong, and B. Lee, "Characteristics of short-period blazed fiber Bragg gratings for use as macro-bending sensors," *Appl. Opt.*, vol. 41, pp. 631–636, 2002.
[11] *Fiber Optic Sensors*, F. T. S. Yu and S. Yin, Eds. Boca Raton, FL: CRC Press, 2002.
[12] L. Higuera and J. Miguel, *Handbook of Optical Fiber Sensing Technology*. New York: Wiley, 2002.
[13] K. Zhou, A. G. Simpson, X. Chen, L. Zhang, and I. Bennion, "Fiber Bragg grating sensor interrogation system using a CCD side detection method with superimposed blazed gratings," *IEEE Photon. Technol. Lett.*, vol. 16, pp. 1549–1551, 2004.
[14] K. V. Madhav and S. Asokan, "Spectrum estimation by wavelength shift time-stamping in a fiber Bragg grating sensor," *IEEE Photon. Technol. Lett.*, vol. 16, pp. 1355–1357, 2004.
[15] M. D. Todd, G. A. Johnson, and B. L. Althouse, "A novel Bragg grating sensor interrogation system utilizing a scanning filter, a Mach-Zehnder interferometer and a 3×3 coupler," *Meas. Sci. Technol.*, vol. 12, pp. 771–777, 2001.
[16] C. Chen, C. Caucheteur, P. Megret, and J. Albert, "The sensitivity characteristics of tilted fibre Bragg grating sensors with different cladding thicknesses," *Meas. Sci. Technol.*, vol. 18, pp. 3117–3122, 2007.

Somayyeh Rahimi received the B.Sc. degree in physics at Sharif University of Technology, Tehran, Iran, the M.A.Sc. degree in electrical and computer engineering from the University of Waterloo, Waterloo, ON, Canada.

She was a Visiting Student at the Institute for Microstructural Sciences, National Research Council of Canada, Ottawa, ON, Canada, from Sept. 2007 and April 2008, where she worked on a fiber Bragg grating sensor project.

Dayan Ban (M'02) received the B.S. and M.S. degrees, both in physics, from the University of Science and Technology of China, Hefei, China, in 1993 and 1995, respectively, and the Ph.D. degree in electrical and computer engineering from the University of Toronto, Toronto, ON, Canada, in 2003.

During 2001–2002, he was a Visiting Scientist at Nortel Networks Optical Components, Ottawa, ON, Canada. In September 2002, he joined the Institute for Microstructural Sciences, National Research Council, Ottawa. He is currently an Assistant Professor in the Department of Electrical and Computer Engineering, University of Waterloo, Waterloo, ON, Canada. Since January 2009, he has been on sabbatical leave from the University of Waterloo and has joined the Research Laboratory of Electronics, Massachusetts Institute of Technology (MIT), Cambridge, MA, as a Visiting Scientist. He has over 80 publications. His research interests include quantum optoelectronic devices, scanning probe microscopy, nanofabrication, infrared LEDs, photodetectors and up-converters, fiber Bragg grating sensors, and Terahertz quantum cascade lasers.

Gaozhi (George) Xiao received the Ph.D. degree from Loughborough University of Technology, Loughborough, U.K., in 1995.

He is currently a Senior Research Officer at the Institute for Microstructural Science, National Research Council of Canada. Ottawa, ON, Canada. He is also an Adjunct Professor at Carleton University. His research work mainly focuses on the development of sensor systems for aerospace applications and building air quality monitoring, as well as the development of flexible transparent electrodes.

Prof. Xiao is an Associate Editor of the IEEE TRANSACTIONS ON INSTRUMENTATION AND MEASUREMENTS.

Zhiyi Zhang received the polymer Ph.D. degree in 1990 from Zhongshan University, Guangzhou, China.

From 1990 to 2001, he was with Zhongshan University, Loughborough University (U.K.), McMaster University (Canada), National Research Council Canada (NRC), Woodbridge Group Company (Canada), and Zenastra Photonics, Inc. (Canada). Since 2002, he has been a Research Officer at NRC. His current research at NRC is focused on microfluidics, photonic sensors, and photonic materials.

Jacques Albert received Physics degrees from the Université de Montréal, Montréal, QC, Canada, and Laval University, Quebec, Canada, and the Ph.D. degree in electrical engineering from McGill University, Montréal, in 1988.

He has held the Canada Research Chair in Advanced Photonics Components at Carleton University since 2004. Prior to his appointment at Carleton University, he had R&D positions with Alcatel Optronics Canada and with the Communications Research Center of Canada. He is coauthor of over 150 publications in journals and conference proceedings and is co-inventor on three patents (and several patent applications).

Dr. Albert has served on or chaired the Technical Committee of several photonics related conferences including the OSA Topical Meeting on Bragg Gratings, Photosensitivity and Poling, Photonics North, CLEO, and the IEEE Photonics Society Annual Meeting. He is currently an Associate Editor for *Optics Express*.